On the Conformational Transitions of Native Xanthan

Leon Bezemer, Job B. Ubbink, Jos A. de Kooker, Maxim E. Kuil, and Jaap C. Leyte*

Department of Physical and Macromolecular Chemistry, Gorlaeus Laboratories, Leiden University, P.O. Box 9502, 2300 RA Leiden, The Netherlands

Received May 6, 1993; Revised Manuscript Received July 26, 1993®

ABSTRACT: Potentiometric titrations of aqueous solutions of *native*, biochemically purified xanthan are analyzed using Henderson-Hasselbalch plots. In addition to the well-known sigmoidal conformational transition, a new consecutive and more gradually evolving conformational transition is observed at low ionic strength and elevated temperatures. As far as we are aware, this transition has not been reported earlier. Rotational viscosity experiments confirm that the first transition induces a severe reduction of the relative viscosity, but the second transition causes a more dramatic change in the viscosimetric behavior: the well-known shear-thinning effect vanishes in the shear rate range investigated. This result shows the inequality of the final states after the first and the second transitions and demonstrates the necessity for the application of a three-state model. Combining the titration results with optical rotation and titration data from the literature, we prove the similarity of the first transition for native and sonicated xanthan. An empirical relation between the midpoints of the first transition, T_m and θ_m, is established which helps to predict the occurrence of a melting point of xanthan solutions at various temperatures and degrees of dissociation.

Introduction

Native xanthan is the high molecular weight ($\approx 10^7$ Da) anionic polysaccharide which is produced by fermentation of the plant pathogen bacterium *Xanthomonas campestris*.[1] The cellulosic backbone is substituted with a trisaccharide side chain at every second residue.[2,3] The degree of dissociation of the side chain carboxylic acid groups can be controlled in a titration experiment. The degree of acetyl and pyruvic acetal substitution depends on fermentation and processing conditions.[4] A major drawback of the commerically available samples is the presence of debris due to postfermentation treatments. Jeanes[1] and later Holzwarth[5] developed a purification procedure based on precipitation of the polymer. In a paper by Whitcomb, Ek, and Macosko,[6] the persistence of protein and DNA after applying this procedure is reported. We developed a new purification method based on treatment with the enzyme DNase followed by phenolic extraction.[7,8] This purification does not influence the molecular weight as checked with LALLS, GPC, and viscosity experiments. With CD spectroscopy a qualitative assessment of DNA and protein impurities can be made. The isodichroic points at 225 and 255 nm in the CD spectra published by Morris et al.[9] can now be assigned to the temperature dependence of physicochemical properties of both xanthan and protein-like impurities and show the sensitivity of this method for the detection of impurities.

Although the primary structure of xanthan could be elucidated independently by Jansson et al.[2] and Melton et al.,[3] the secondary structure or conformation is still a matter of debate. In the first publications on xanthan, Jeanes et al.[1] reported the physicochemical behavior of aqueous xanthan solutions with evidence for a conformational transition. From X-ray scattering experiments, Moorhouse et al.[10] initially postulated a single-helix model, but in a second paper[11] these data were combined with the density of the sample, and a double helix with a pitch of 47 Å per repeat unit of 10 monomers was postulated. From electron microscopy experiments, Holzwarth et al.[12] concluded that multiple stranded structures can exist, while Stokke et al.,[13] using a highly pyruvated sample, observed a variety of strands depending on the initial salinity of the samples. With a variety of techniques, such as viscosity, ORD, CD, NMR, LALLS, and DSC,[1,5,9] a temperature dependence can be observed which is interpreted as a conformational transition. It is usually assigned to the melting of a helix, but none of the techniques has thus far solved the single/double/multiple-helix controversy. The perfectly matched single- and double-helix models lead to factor of 2 difference in the mass per length and charge density parameters. But if these models are applied to experimental results, an inconsistent picture emerges. Both the single- and double-helix models are supported by experiments, and sometimes the results are inconclusive. For instance, Milas et al.[14] applied the condensation concept to a temperature-dependent conductance experiment. They concluded that the single-helix-to-coil transition which induces a decrease of counterion condensation is in accord with the observed changes of the conductance.

In calorimetric experiments, Norton et al.[15] and later Paoletti et al.[16] applied the relation between the midpoint of the transition, T_m, and the fraction of condensed counterions.[17] While Norton et al. rejected a double-stranded structure, Paoletti et al. rejected a single-stranded structure using the same relation.

Contradictions arise not only between different experimenters but also in different experiments by the same authors. Norton et al. obtained a reduction of M_w by a factor of roughly 2 in a LALLS experiment, which is generally taken as evidence for the double-helix model, while in an optical rotation experiment single-order kinetics was observed for the conformational transition rate, indicative for a single-helix model. With our results this first-order kinetics may be ascribed to the intramolecular process of the unfolding of side chains. It is obvious that incorporation of imperfections such as imperfect matching, loops, or cluster formation in the "perfect" helix models should be taken into account, and indeed some experimental evidence is given by the electron microscopy results of Stokke et al.[13] Norton et al. referred to the model proposed by Rees[18] which involves a side-by-side aggregation mainly leading to dimers of single helices. The decrease of M_w upon heating could be explained by a dissociation of such aggregates or clusters, while the results from calorimetric and optical rotation experiments cor-

® Abstract published in *Advance ACS Abstracts*, November 1, 1993.

0024-9297/93/2226-6436$04.00/0

respond with the single-helix character. The mass per length parameter which has been determined by several authors also has a limited significance. Albeit the perfect single- and double-helix models lead to values of ca. 1000 and 2000 Da/nm, respectively, a contamination of these figures is expected if imperfections cannot be neglected. However, in the literature[19-21] the most abundant value of the mass per length for the ordered state of both native and sonicated samples is ca. 2000 Da/nm, which seems to indicate some average strandedness of two.

In an extended series of experiments, Sato, Sho, Liu, Fujita, Norisuye, and co-workers[22-27] investigated the ordered and disordered conformations of sonicated, i.e., low molecular weight, xanthan samples in aqueous and acidic HCl solutions with 0.01–0.1 M NaCl added. They conclude that a partial rupture of a double-stranded structure takes place going from 25 to 80 °C since the persistence length diminishes from ≈1000 to ≈250 Å, but the molecular weight is invariant throughout this range. These authors also compared the LALLS results of xanthan in aqueous solution with those of xanthan in the solvent cadoxen and concluded that xanthan is double stranded. We wish to comment on this reasoning that, in the solvent cadoxen, xanthan may be severely deformed by interaction with the bivalent cadmium ions, which may invalidate an exact comparison with the aqueous solution.

Lecourtier et al.[28,29] reported the salt concentration dependent molecular weight variation of a fully pyruvated xanthan species, indicative for a salt-induced conformational transition. The electrostatic repulsion for this fully pyruvated sample is a driving force for the transition at temperatures where low-pyruvated samples are inert. These authors also noticed irreversible changes in optical rotation when the ionic strength of the xanthan solution was decreased and successively increased. An irreversible rearrangement of hydrogen-bonded structure in a double helix was suggested by the authors, although an equally probable explanation is offered by the Rees model. Some gradual dissociation process of clusters with an average strandedness of two may also cause the observed reduction of M_w and time dependencies.

The difficulty in defining the true equilibrium for xanthan solutions is also illustrated by the findings of several other authors[5,26,30-33] who report time dependencies and "hysteresis" effects on various time scales in viscosity, light scattering, and optical rotation experiments. In most cases deviations from reversibility are observed if "fresh" samples are being used. At this point we would like to report the outcome of several of our unpublished experiments that for equilibration, freshly dissolved xanthan should be stirred for several weeks. In a simple optical rotation experiment, the "hysteresis"-free sigmoid transition results from the literature could only be reproduced after several attempts, while the original xanthan solution had aged a few weeks. In a forthcoming paper we will report NMR measurements from which an equilibration time of 7 weeks can be deduced.[34] Another problem is posed by the formation of anisotropic phases due to the stiff nature of the polymer. The intrinsic persistence length is roughly 1000 Å,[21-26] and, consequently, a calculation using Odijk's formulas[35] shows that at any concentration above c^* the total persistence length exceeds the correlation length of the lattice of overlapping chains. Consequently, this lattice does not melt—i.e., c^{**} is never approached—and anisotropic domains are formed. From birefringence experiments, the onset of the formation of liquid crystalline phases is estimated to take place below 10 g/L, with some authors claiming as low as 3 g/L.[30,31,36,37] The study of conformational transition effects should take place in a concentration range which is below the phase separation concentration. The phase diagram must therefore be investigated and the upper bound of the isotropic phase must be assessed. In this laboratory it was shown[38] that ^{23}Na NMR relaxation measurements provide a very sensitive test for deviations from isotropy in solutions of DNA. With the use of this technique we have determined[34] the upper bound of the isotropic phase and the onset of LCP formation, which equals 5 g/L for our xanthan sample without added salt.

The NMR relaxation rates of the ^{23}Na counterions of xanthan samples could also be used to follow the equilibration process in a freshly prepared solution. The relaxation rate of a sample which had been rapidly concentrated beyond the concentration at which phase separation takes place in a rotatory evaporator at 30 °C and 15 mmHg decreased during the following 50 days and remained constant over the next 850 days. As far as the authors know, this is the first experiment in which the equilibration time of a native xanthan solution near the phase transition concentration is set at 50 days. Also, this demonstrates the stability of xanthan over a 2-year period after equilibration.

Our observations seem to agree with the findings of Carnali,[33] who investigated the rheology of xanthan solutions near the phase transition and concluded that long-term equilibration processes take place. Once a method is known to define equilibrium, the conformational transition can be studied. From all the studies up till now, most experiments were carried out by increasing the temperature and monitoring the changes. In only a few experiments, the transition was induced by titration, i.e., gradually increasing the charge on the polymer. In both types of experiments, the polymer is taken away from equilibrium gradually and is observed. The essential point is that the polymer should not be driven too far from equilibrium. In our view, many observations of hysteresis and slow relaxation effects in *temperature*-dependent optical rotation studies seem to indicate either that the solution had not been properly equilibrated or that indeed the polymer may be too far from equilibrium in such experiments. On the other hand, in titration experiments which are carried out under isothermal conditions, the polymer is perhaps driven only slightly off equilibrium if small doses and large increment times between the doses are being used. Indeed no such "hysteresis" problems seem to occur in several titration studies in which the conformational transition can be observed.[39-41] Titrations can be analyzed using a Poisson–Boltzmann approach, and the result of such an analysis is that the description of the conformational transition in terms of the dissociation of a double helix into single helices fails.[40] This result supports the generally adopted hypothesis that the sigmoid transition is not a true dissociation of dimers.

In a titration experiment one measures the chemical potential of the protons, which is related to the charge density of the polyelectrolyte through the pK_a of the acidic groups. A conformational transition influences the charge density parameter, and this results in a peculiarity in the titration curve. In the cases of PMA[42] and xanthan,[39,41] a minimum in the pK_a versus θ curve is observed. For PMA it was concluded from these observations that a transition takes place from a highly coiled to a less densely coiled structure. In a similar way one may conclude that xanthan is also transformed into a structure of smaller charge density. In this paper we analyze the salt and temperature dependence of the potentiometric titration

curves of xanthan to further investigate the transition when the polymer is taken away not too far from equilibrium and propose a model consisting of two conformational transitions: the first transition from state A to B and the second from state B to C. The results of the first transition are compared with a study of Nakasuga et al.[41] on sonicated xanthan. We would like to stress that the comparison with sonicated samples is allowed only for samples of a contour length exceeding the Kuhn length in accordance with the observed molecular weight independence of the optical rotation for samples of M_w larger than $\approx 4 \times 10^5$ reported by Liu et al.[26]

Experimental Section

Purification Procedure. Commercial food grade Keltrol T (Kelco, lot no. 370109V, a kind gift of Danby Chemicals, Amsterdam) was used. Elemental analysis of this product shows the presence of at most 4.1% protein (0.65% N) and 1.4% DNA (0.13% P). The presence of protein and DNA was qualitatively confirmed by Coomassie Brilliant Blue staining and ethidium bromide fluorescence tests, respectively.[43,44] All manipulations were carried out at ca. 23 °C. The polymer was dissolved in 7 L of a 0.1 N NaCl/6mM NaN_3 aqueous (milliQ, Millipore) solution to a concentration of 4 g/L. To improve solubility and homogeneity, this solution was rigorously stirred for 3 weeks with a glass blade propeller at such a rate that a rod-climbing effect was observed. To this solution, Tris (tris(hydroxymethyl)aminomethane), $MgCl_2$, $CaCl_2$, and NaH_2PO_4 were added to concentrations of 40, 6, 2, and 5 mM, respectively, and the pH of the solution was adjusted to 7.00 with 0.1 N NaOH. To the solution at rest was added 140 μL of DNase I (Boehringer, bovine pancreas grad II), and the following 2 days the solution was stirred very gently. In a preliminary experiment it was checked that incubation with the DNase did not affect the viscosity of the solution. The solution was divided in several portions and extracted with a phenol/chloroform/isoamyl alcohol (w/v 25:24:1) mixture.[7,8] The extracts were centrifuged at 2500 rpm for 15 min in portions of 0.5 L. The aqueous layers were extracted twice with a chloroform/isoamyl alcohol (w/v 24:1) mixture and centrifuged. The combined supernatants were dialyzed three times against a fivefold excess of 0.1 N NaCl/5 mM EDTA to dispense with the bivalent ions and to restore the NaCl concentration. The combined solutions were ultrafiltrated using a Millipore Minitan equipped with M_w 400 000 cutoff filter plates to remove residual small impurities and to increase the polymer concentration. A test[45] with the complexating agent Vantocil 1B confirmed the absence of xanthan in the filtrate. The overall yield of purified xanthan is roughly 50% due to losses presumably caused by the imperfect separation of layers after centrifugation and by adsorption on the filter plates. The stock solution of purified xanthan in 0.1 N NaCl was stored at 4 °C after addition of 50 ppm NaN_3.

Characterization of the Purified Xanthan Sodium Salt. The purification procedure was monitored by circular dichroism (CD) spectrocopy using a modified Cary 61 spectropolarimeter.[46] The OD of the solutions was measured with a Cary 219 UV spectrophotometer. In Figure 1 the CD spectra are shown of the xanthan solutions: before purification (1), after DNase treatment (2), after DNase treatment/phenolic extraction (3). The spectra are corrected for the differences in xanthan concentration, determined with a carbon analyzer.

Although the molar ellipticities of the DNA and protein impurities are unknown, the spectra indicate that the major impurity is protein. The strong curvature of spectra 1 and 2 toward the base line, in contrast with spectrum 3, indicates that the purification improves the solution homogeneity with a concomitant decrease of differential scattering, in agreement with the OD spectra.

The purification reduces the protein content to roughly 1% (20% of its initial value according to CD). The values of the DNA content before and after the purification are 0.8 and 0.2%, respectively, obtained from a quantitative ethidium bromide fluorescence test. The purification reduces the protein content by a factor of 5 and the DNA content by a factor of 4 on this scale.

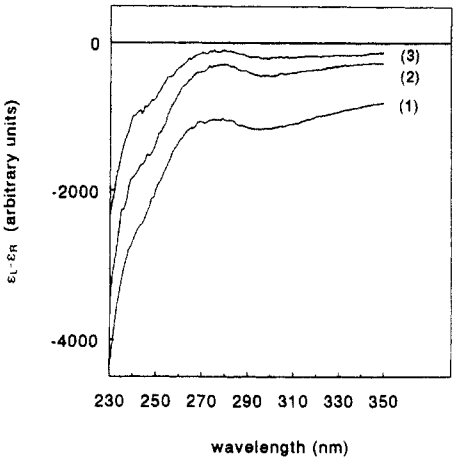

Figure 1. Circular dichroism spectra: spectrum 1, unpurified xanthan; spectrum 2, DNase-treated xanthan; spectrum 3, DNase/phenolic extraction-treated xanthan. Spectra are given in arbitrary units. C_p = 2.30, 2.28, and 1.69 g/L (2.51, 2.49, and 1.85 mM) for the solutions of spectra 1, 2, and 3, respectively.

After dialysis and ultrafiltration, the residual calcium concentration was determined with a Perkin-Elmer 460 atomic absorption spectrometer. A value of less than 10^{-7} M was obtained, which corresponds to less than 0.01% of the monomer concentration.

The fractions of acetyl and pyruvic acetal substitution per monomer, D_{ace} and D_{pyr}, respectively, were determined by ^1H NMR spectroscopy at 85 °C using a Bruker WM-300 spectrometer operating at 300 MHz. The xanthan sample was exchanged with D_2O repeatedly, and hydroquinone was added as an internal reference. The fractions of substituents are not influenced by the purification process: $D_{ace} = 0.8 \pm 0.1$ and $D_{pyr} = 0.5 \pm 0.1$.

The optical rotation of purified xanthan in 3×10^{-3} M NaCl was measured with a Perkin-Elmer 214 spectropolarimeter operating at 365 nm. The value of $T_m = \pm 45$ °C at this ionic strength agrees with the data published by Norton et al.[15] on native xanthan and with the data of Liu et al.[26] on sonicated xanthan.

The molecular weight M_w of a concentration series in 0.5 M NaCl was determined with LALLS on a Chromatix KMX-16. The refractive index increment was determined with a Chromatix KMX-6 laser differential refractometer, and the value of 0.149 mL/g is in agreement with the results of Hacche et al.[30] The solutions were filtered through 8-μm Millipore filters after centrifugation at 15 000 rpm. Loss of ca. 25% of the material after centrifugation seems to indicate the presence of aggregates or undissolved polymer. The value of the virial coefficient A_2 which is almost zero is in accordance with literature data.[15,30] It is important to stress that the M_w values obtained by the LALLS method are seriously influenced by the filtration prior to the experiment. Depending on filter pore sizes, values of roughly $(2–40) \times 10^6$ Da are obtained.[19] In a recent paper, an M_w value of 36×10^6 was reported after filtration through 0.65-μm pore size.[47] Our value of $(30 \pm 10) \times 10^6$ Da after filtration through an 8-μm Millipore filter agrees quite well with these observations.

Preparation of the Acidic Form and Potentiometric Titrations. The stock solutions were converted into the acidic form by dialysis against ca. 0.03 M HCl (p. a. Merck) for at least 2 weeks. A shorter dialysis time results in an incomplete (±70%) conversion, and an equivalent weight above the theoretical value is obtained by titration. Atomic absorption measurements show that the amount of residual sodium for this intermediately converted species is less than 3% of the equivalent concentration, which is insufficient to account for the missing protons. A similar discrepancy was reported by Sloneker et al.,[48] who proposed a mechanism of lactone formation to account for the difference. The amount of residual sodium in the acidic forms after dialysis for 2 weeks is less than 0.1% of the carboxyl group concentration as determined with a Perkin-Elmer 460 atomic absorption spectrophotometer. The possible role of lactone formation is currently under investigation in this laboratory.

The titration experiments were run on a Radiometer VIT90 titrator equipped with a 1-mL autoburet station. The temperature of the titration vessel was controlled by a circulating-water bath, and the solution was vigorously stirred with a magnetic stirrer. To prevent evaporation and the absorption of CO_2 during the experiment, a blanket of nitrogen gas saturated with water vapor isothermal to the solution was delivered to the titration atmosphere. The pH was measured with a Radiometer GK2401C combined glass–calomel electrode with a KCl contamination rate into the titration vessel of 5×10^{-5} M/h. The electrodes were calibrated at the same temperature as the solution with the Radiometer and Merck pH 4.00 and 7.00 standard buffers. The delay time between successive additions of titrant was increased until this value no longer influenced the results. A delay time of 6 min between additions of 0.07 mL of titrant was necessary to provide equilibrium conditions. The titrations typically spanned 14 h. The contamination of salt from the electrode near the point of equivalence is on the order of 0.5 mM. Screening of the conformational transition effects due to this low level of contamination can be neglected. The degrees of dissociation were determined from the end points of the titrations and corrected for changes in volume and the water autodissociation, calculated from K_w at all temperatures.[49]

Determination of the Xanthan Concentration. The most laborious method is to determine by IR spectroscopy the water content of a lyophilized xanthan sample dissolved and exchanged in D_2O. At least 40 mg of lyophilized xanthan is needed to avoid inaccuracy in the weighing of the material, which is not easy to handle.

A more routine method is to determine the amount of total organic carbon (TOC) with an Ionics 1555B carbon analyzer capable of handling all ionic strengths. In practice, only 50 μL of xanthan solution per analysis is needed, and a reproducibility of 1.5% is accomplished with ca. 10 tests. The carbon content of a xanthan monomeric unit depends on the degrees of substitution of acetyl and pyruvic acetal groups and of the degree of dissociation, θ. From the primary monomeric structure we derived an expression for the carbon content. An error analysis shows that with $D_{ace} = 0.8 \pm 0.1$, $D_{pyr} = 0.5 \pm 0.1$, and θ known with an accuracy of ±0.1 the carbon content is $((44.4 - 1.5\theta) \pm 0.6)\%$. The theoretical accuracy is then 1.4%. With this method, monomeric concentrations could be determined with an overall accuracy of 2–3%. The unit for the concentrations of the polymer solutions will be denoted mM, which is shorthand for milli-*mono*molar.

Viscosimetry. Rotational viscosity measurements were performed with a Haake RV 20 rotovisco/RC 20 rheocontroller equipped with a CV 100/ME 30 measuring probe and thermostated using a Braun Thermomix B4 water thermostat. The equipment was calibrated with a temperature series of isoamyl alcohol with known viscosity.[50] For brevity in presentation, a selection was made of the data corresponding with shear rates of 10, 20, 40, 100, and 300 s^{-1}.

Results

Potentiometric Titrations and Viscosimetry Data. In Figure 2 the titration curves of xanthan solutions at different temperatures are presented. The polymer and salt concentrations are 2.06 mM (1.89 g/L) and 0.5 mM, respectively. If the temperature is increased, the conformational transition becomes more pronounced.

The addition of salt has a well-known quenching effect on the transition, which is also demonstrated in Figure 3, where pK_a versus θ at 63 °C is given at several ionic strengths. In addition to the potentiometry, the rotational viscosity of samples with different degrees of dissociation was measured as a function of the temperature to compare the pK_a changes to changes in the viscosity. At lower temperatures and degrees of dissociation (not shown) a pronounced shear thinning is observed as usual[1,5] for the "ordered state"; i.e., if the shear rate is increased, the viscosity decreases. However, at the highest degree of dissociation this well-known effect readily disappears

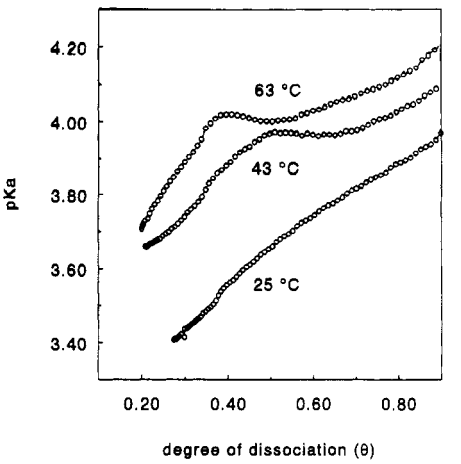

Figure 2. Plot of pK_a versus θ at three temperatures and C_s = 0.5 mM: 63, 43, and 25 °C are shown (results for 53 °C are omitted for clarity). C_p = 1.89 g/L (2.06 mM).

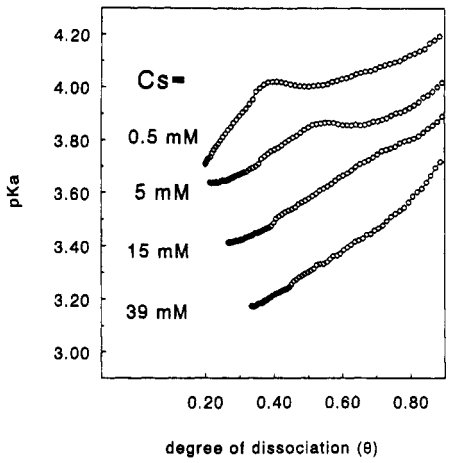

Figure 3. Plot of pK_a versus θ at 63 °C with added salt: C_s = 0.5, 5, 15, and 39 mM, respectively. C_p = 1.89 g/L (2.06 mM).

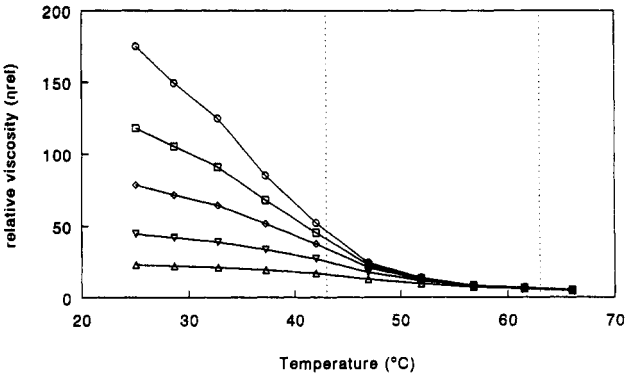

Figure 4. Relative viscosity at various temperatures as a function of the shear rate. The degree of dissociation, θ, for this sample is 0.9. At 43 °C (dotted line), $f_A = 0$ and $f_B = 1$; at 63 °C (dotted line), $f_A = 0$, $f_B < 0.1$, and $f_C > 0.9$. Shear rates are 10 (○), 20 (□), 40 (◇), 100 (▽), and 300 s^{-1} (△) from top to bottom. Beyond roughly 60 °C, going from 10 to 300 Hz the relative viscosity decreases less than 5%, which is inside the experimental accuracy. At 43 °C the relative viscosity decreases a factor of 3 going from 10 to 300 Hz. C_p = 2.6 g/L (2.84 mM).

beyond 60 °C; cf. Figure 4. Thus the conformational transition not only leads to a severe decrease of the viscosity, which is well documented in the literature,[1,5,41] but at a certain point the characteristic shear-thinning effect vanishes for the present shear rate range, which has not yet been reported in the literature. The disappearance of this effect clearly indicates the change of the nature of the polymer. If 5 mM salt is added, then the shear-thinning

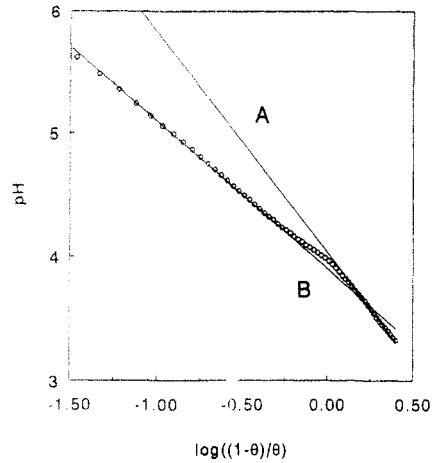

Figure 5. Henderson–Hasselbalch plot at 43 °C. Branches of A and B of the linear regressions are drawn (see text). Regression of A for $0.33 < \theta < 0.41$, correlation coefficient = 0.9955 (nine data points); regression of B for $0.71 < \theta < 0.78$, correlation coefficient = 0.9986 (six data points). C_p = 1.89 g/L (2.06 mM).

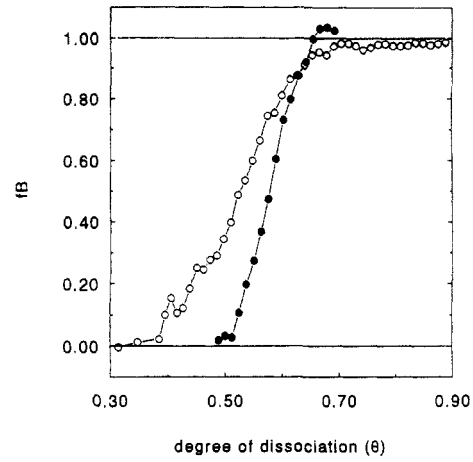

Figure 6. Development of the molar fraction of B in the course of the titration: composition curve of f_B at 43 °C and C_s = 0.5 mM (○) and 63 °C and C_s = 5 mM (●), respectively; C_p = 1.89 g/L (2.06 mM).

effect is restored at temperatures up to 65 °C. The shear-thinning effect then vanishes again beyond ~70–75 °C.

With use of the results of the next section from the composition curves of Figures 6 and 10 we have calculated the molar fractions of A, B, and C in the cases 43 and 63 °C indicated in the viscosity plot of Figure 4. In the former case, $f_A = 0$ and $f_B = 1$ while in the latter case, $f_A = 0$, $f_B < 0.1$, and $f_C > 0.9$.

Henderson–Hasselbalch Analysis of the Titrations. To proceed with an analysis of the titrations, we will turn to the so-called Henderson–Hasselbalch method which has been used earlier to describe the conformational transition of PMA.[42] For further details the reader is referred to the section "Henderson–Hasselbalch Calculations". In this analysis it is somewhat naively assumed that the initial and final linear branches of the Henderson–Hasselbalch curve can be associated with the pure states "A" and "B". In the composition curve which follows from the analysis the conversion to B is scaled from 0 to 1, intrinsic to the AB method.

In Figure 5 the Henderson–Hasselbalch plot is shown for the case 43 °C/C_s = 0.5 mM. The drawn lines are the linear regressions of the initial and final branches of this plot. The data points for which the calculated value of θ was almost completely determined by the pH (i.e., for θ less than ca. 0.34) were omitted from the regression. Figure 6 shows the development of B in the course of the titration as a typical example of the sigmoid transition profiles which are well-known from, e.g., optical rotation studies. In Figure 7 the development of B in the course of the titrations at T = 25, 53, and 63 °C is shown for C_s = 0.5 mM. These curves deviate from the "normal" sigmoid shape of 43 °C; cf. Figure 6. For instance, at the lowest temperature (25 °C) it seems as if the transition is not yet complete, since apparently only the lower half of the s-shaped curve is observed. Intrinsic to the AB method the conversion to B is scaled from 0 to 1, but the final conversion may be less than 1 if the final branch corresponds to some intermediate state between A and B which is almost invariant during the last part of the titration. This result indicates that the first transition can proceed gradually, either by increasing the degree of dissociation or by increasing the temperature, a feature which is consistent with several observations of the optical rotation in the literature in which temperature or degree of dissociation is gradually increased.[9,26,39]

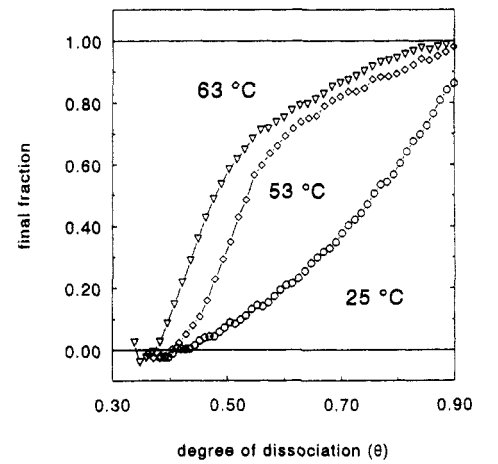

Figure 7. Composition curves at 25, 53, and 63 °C, C_s = 0.5 mM. Molar fraction of final state plotted as a function of θ. C_p = 1.89 g/L (2.06 mM).

In addition to the rather steep s-shaped curve, a more gradual process is observed beyond 43 °C. This process is easily quenched by the addition of salt; cf. Figure 6 in which the case 63 °C/C_s = 5 mM is inserted: again a "normal" sigmoid-shaped curve is obtained. Comparison of Figures 6 and 7 shows that at low salt concentration the two-state model is inadequate whereas it is satisfactory at $C_s \geq 5$ mM. As most previous work has been done at higher salt concentrations, this explains why the presently reported irregular behavior has not been observed before. The AB model failing, the simplest possible extensions are either a second type of reaction, initiated in a later stage of the titration and also leading to the B state, or a second transition of B to some state C can be introduced. The essential issue is that in the latter case a clear difference of the physical properties of the B and C states must be demonstrated. If not so, then two different processes generated at different degrees of dissociation or temperatures, both leading to physically indistinguishable B states, may be at work. To make the proper choice, the viscosity results need further scrutiny.

To summarize, the following parallel observations are made in the potentiometric titration and the rotational viscosity experiments. At low concentrations of added salt, a sigmoid transition is observed with conservation of shear-thinning up to ca. 43 °C. At temperatures beyond 43 °C, a second process is observed which readily cancels the shear-thinning effect. The addition of 5 mM salt

Table I. Results of the Henderson–Hasselbalch Analyses of the Two-State (AB) and Three-State (ABC) Cases

T (°C)	C_s (mM)	n_A	pK_0^A	n_B	pK_0^B
25	0.5	1.71	3.68	1.49	3.44
43	0.5	1.79	4.03	1.20	3.90
63	5	1.47	3.85	1.24	3.79

T (°C)	C_s (mM)	n_A	pK_0^A	n_B	pK_0^B	n_C	pK_0^C
53	0.5	1.80	4.05	*a*		1.28	3.82
63	0.5	1.79	4.19	1.29	3.97	1.32	3.90
73	0.5	1.69	4.10	*a*		1.46	3.69

[a] The concentration of B cannot be determined.

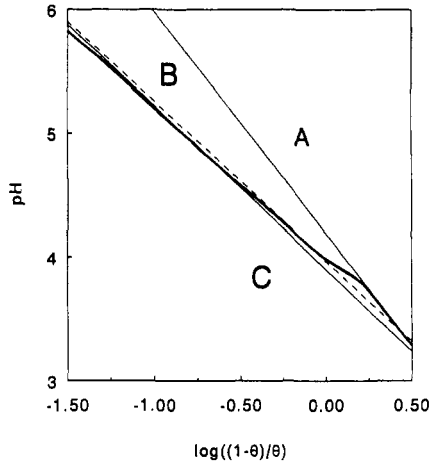

Figure 8. Henderson–Hasselbalch plot at 63 °C with C_s = 0.5 mM (solid curve). A and C are the branches of the initial and final states A and C, obtained by linear regression (straight lines). B is the branch of the intermediate species B, obtained by an iterative procedure (dotted line). C_p = 1.89 g/L (2.06 mM).

quenches both the second process and the cancellation of a shear-thinning effect, at least up to ~70–75 °C; i.e., the addition of salt shifts the occurrence of the second transition to higher temperatures. The physicochemical difference between the final states after the first transition (shear thinning) and the second process (no shear thinning) is hereby shown, and hence we can adopt the ABC type model to account for the case of 63 °C and C_s = 0.5 mM.

Then, of course, our naive "AB" assumption in the Henderson–Hasselbalch analysis is erratic for temperatures exceeding 43 °C. The final branch in these cases will correspond with some state C. As a consequence, the composition curves of Figure 7 are erroneous to the same extent. The analysis may however be improved as follows. Since the B state is an intermediate state in these titrations, we can try to estimate the branch of this B state in the Henderson–Hasselbalch plots. In the section "Henderson–Hasselbalch Calculations", an iterative method is described to obtain a consistent linear regression of a Henderson–Hasselbalch branch of the intermediate B state, and in addition expressions for the composition curves of the ABC cases are derived. In Table I the results are shown of the linear regressions of the Henderson–Hasselbalch plots including the iterated solution for B at 63 °C.

The result of the iterative process is shown in Figures 8–10. Two solutions of the iteration were found, of which only one, shown in Table I, was fully consistent with the boundary conditions; cf. the section "Henderson–Hasselbalch Calculations". The result of the iterated Henderson–Hasselbalch regression for the B species is shown in Figure 8.

Since thermodynamic equilibrium holds for every value of θ, we can calculate the conformational equilibrium constants K_1 and K_2, which are given by the ratios [B]/[A] and [C]/[B], respectively, at fixed values of θ. In the theoretical section we will explain that K_i is a function of θ. In Figure 9 the dependence of $\ln(K_i)$ on θ and the linear regressions are shown. From this figure in fact the midpoints of the first and the second transitions, θ_{m1} and θ_{m2} can be derived from the θ for which $\ln(K_i) = 0$. There is a great difference between the two processes; the dependence of $\ln(K_i)$ on θ for the second transition is less steep. In Figure 10 the development of A, B, and C is shown. It is seen that the B species does not become a pure intermediate state; by the time it has grown to roughly 90%, it is significantly transformed into C; cf. the dotted line of Figure 10. The two processes are clearly coupled but nevertheless at the beginning and the end of the titration one single transition dominates, given the behavior of $\ln(K_1)$ and $\ln(K_2)$ of Figure 9 and the stoichiometry of Figure 10.

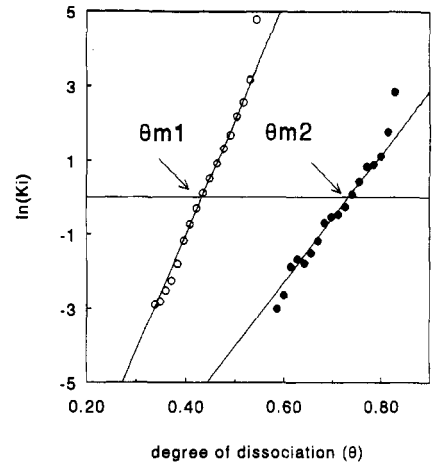

Figure 9. $\ln(K_i)$ versus θ at 63 °C and C_s = 0.5 mM; final solution of iterations. Linear regression enables the extrapolation of ln K_1 (○) and ln K_2 (●) as a function of θ. C_p = 1.89 g/L (2.06 mM). The arrows indicate the midpoints of the first and the second transitions: θ_{m1} and θ_{m2}.

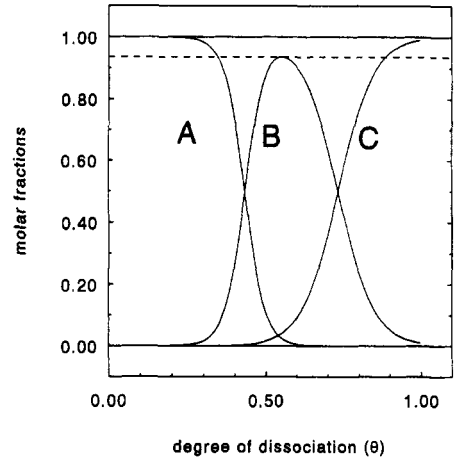

Figure 10. Development of A, B, and C in the course of the titration at 63 °C and C_s = 0.5 mM; final solution of the iterative method. The dotted line indicates the maximum conversion to B (0.93). C_p = 1.89 g/L (2.06 mM).

In Table II the linear regression results of $\ln(K_i)$ versus θ are shown for all of the AB cases and also the ABC case at 63 °C. In the AB cases the transitions are described by $\ln(K_1) = C_1\theta - C_2$, and in the ABC case an additional regression of $\ln(K_2) = C_3\theta - C_4$ is made. For $\ln(K_i) = 0$ a midpoint of transition can be defined: $\theta_{m1} = C_2/C_1$ and $\theta_{m2} = C_4/C_3$.

An Empirical Correlation between T_m and θ_m. From the composition curves of Figures 6, 7, and 10 and the use

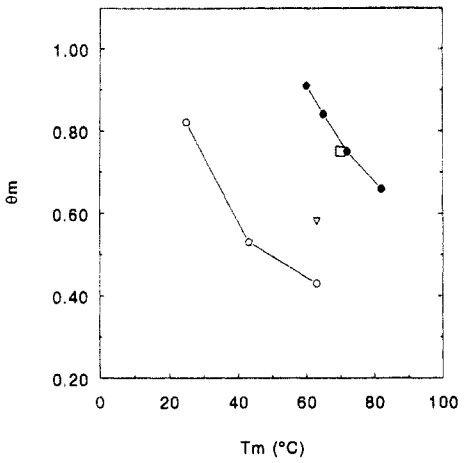

Figure 11. Correlation diagram of T_m and θ_m at various concentrations of added salt. Lines are drawn as an aid to the eye. (○) Titration results at C_s = 0.5 mM and C_p = 1.89 g/L (2.06 mM); (▽) titration result a C_s = 5 mM and C_p = 1.89 g/L (2.06 mM); (●) optical rotation results of Nakasuga et al.[41] at C_s = 10 mM and C_p = 1.65–1.73 g/L. Open square (□) close to closed circles (●) is an extrapolation of the titration results to C_s = 10 mM.

Table II. Linear Regression Results of $\ln(K_i)$ versus θ: Determination of the Midpoints of the Transitions

T (°C)	C_s (mM)	θ_{m1}	θ_{m2}
25	0.5	0.82	
43	0.5	0.53	
63	0.5	0.43	0.73
63	5	0.58	

of Table II we can construct a correlation diagram of the two parameters which determine the midpoint of the first transition, T_m and θ_m, at a fixed salt concentration of C_s = 0.5 mM; cf. Figure 11. For all of the data points in this figure, the transition is halfway; i.e., one deals with half-(dis)ordered states. A slightly curved correlation is observed; i.e., the conformational effects due to the addition of electrostatic and thermal energy to the system are correlated. For the second transition only one data point is available, and a further analysis is therefore omitted. The obvious feature is that the second transition can be brought about only at higher temperatures. In Figure 11 we inserted data points of Nakasuga et al., obtained from a temperature-dependent optical rotation study of sonicated xanthan[41] ($M_w = 7.44 \times 10^5$) at C_s = 10 mM. A similar correlation is observed and we expect all data points to shift to higher values of T_m and θ_m values since the addition of salt screens the electrostatic interaction. The effect of added salt is to shift the correlation diagrams.

We estimated the shift going from 5 to 10 mM using data of a study of the effect of salt on T_m by Liu et al.[26] and we used our data of the effect of salt on θ_m at 63 °C. The corresponding effects are 7 °C on T_m and 0.17 θ units of θ_m. Thus, the data point 63 °C/5 mM/θ = 0.58 shifts to 70 °C/10 mM/θ = 0.75. This calculated point is inserted in Figure 11, and fair agreement with the correlation diagram at C_s = 10 mM of Nakasuga et al. is obtained. Very close to the calculated point, the experimental point 75 °C/10 mM/θ = 0.72 is available. Nakasuga et al. also published their potentiometric titration data at these conditions.[41]

We will now compare the titration curves to test the validity of such a shift of the correlation diagrams. From our titration experiments (cf. Figure 3) we expect a shift of ca. 0.26 pK_a units going from 5 to 10 mM. The θ axes are shifted by 0.14. In Figure 12 both curves are shown

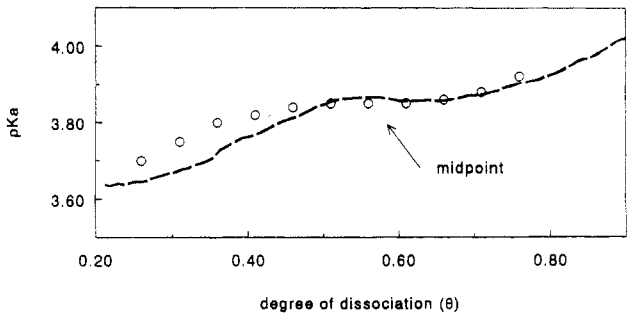

Figure 12. Comparison of shifted titration curves using the correlation diagram of Figure 11. The dashed line represents our original titration data at 63 °C, C_s = 5 mM, and C_p = 1.89 g/L (2.06 mM). The open circles are data of Nakasuga et al., shifted along both the pK_a and θ axes (see text), at 75 °C, C_s = 10 mM, and C_p = 1.49 mM.

and the data of Nakasuga et al. are shifted. The agreement of corrected pK_a's at the "midpoint" indicated in Figure 12 is surprisingly good. Thus, with the above-mentioned proviso it is now shown that our biochemically purified native xanthan shows a sigmoidal first transition behavior identical to the sonicated xanthan of $M_w = 7.44 \times 10^5$; i.e., the sigmoidal or first transition behavior of a sonicated chain made up of ca. 6 Kuhn segments and a native chain made up of ca. 20 Kuhn segments is identical. A direct comparison with literature data is not possible for the second transition.

Reversibility Check of Both Transitions. To investigate the reversibility of transitions observed in titrations, the method of back-titration seems obvious. A major drawback of this method at polymer concentrations as low as 5 mM is that as a result of the neutralization process the salt concentration increases to 5 mM, which is now known to quench the second transition. Since the pK_a changes are quite small, this increase of the salt concentration will inherently cause hysteresis and obscure irreversibility effects. Therefore back-titrations do not provide a feasible test. Instead, we investigated the (ir)-reversibility of the transitions by cyclic changes of the temperature of several samples at different degrees of dissociation with the use of ^{23}Na NMR relaxation, otical rotation, and circular dichroism measurements. In a forthcoming paper[32] we will demonstrate that these relaxation measurements are extremely sensitive to conformational transitions. The results are not discussed in detail here, but suffice it to report that with the NMR and the CD experiments the reversibility of both the first and second transitions within 24 h is established. The irreversibility effects reported in the literature must consequently be ascribed to sample preparations such as applying too short an equilibration time after dissolving the polymer rather than caused by either of the two transitions.

Viscosimetry. We can make a tentative comparison of our viscosity data and some calculations of the persistence length and molar mass per unit contour length of xanthan in the literature. For Na xanthan in 10 mM NaCl solution, the persistence length was found to decrease from ~1200 to ~250 Å, and the mass per unit contour length was found to decrease from 1940–1760 to 760 nm^{-1} upon going from 25 to 80 °C.[25,26] The essential question which follows from our results is: are these strong decreases caused by the first (AB) or the second (BC) transition?

The strong reduction of the persistence length may account for the rather sharp decrease of the relative viscosity, such as observed in Figure 4. At a salt concentration of 5 mM we expect the onset of the second transition

at ~70–75 °C, since the shear-thinning effect vanishes at this point (not shown in the figures). At 10 mM the second transition will be shifted to even higher temperatures, but since the experimental range of these viscosity experiments is limited to 70 °C, no data are available to check the case of 80 °C and 10 mM for the occurrence of the second transition. The second transition drastically changes the viscosity behavior of the polymer, and it would not be surprising if it is accompanied by such large decreases of the persistence length and mass per length parameter as cited above. On the other hand, if the first transition involves the unfolding of the side chains, it is also expected to lead to a decrease of the persistence length. Clearly, more calculations of the persistence length and mass per length are needed in the first transition region, for instance at 63 °C and 5 mM.

Henderson–Hasselbalch Calculations. In an aqueous solution of a weakly acidic polyelectrolyte HA an equilibrium is established between the dissociated protons and the polyanion. The work which is required to remove a proton from a charged macromolecular chain increases with the degree of dissociation θ, and hence the proton dissociation equilibrium "constant" K_a is *not* a constant but a function of θ. The degree of dissociation θ and K_a are given by

$$\theta = \frac{[A^-]}{[HA] + [A^-]} \qquad K_a = \frac{[H^+][A^-]}{[HA]} \tag{1}$$

θ is corrected for changes of volume and the contribution of water dissociation and is calculated from the end point of the titration and the degree of neutralization θ' with the relation

$$\theta = \theta' + \frac{[H^+] - [OH^-]}{C_p} \tag{2}$$

In the so-called extended Henderson–Hasselbalch equation the increment of the electrostatic energy involved in the dissociation process is represented by a constant, n, in eq 3.

$$pH = pK_0 - n \log\left(\frac{1-\theta}{\theta}\right) \tag{3}$$

A Henderson–Hasselbalch plot of the $\log((1-\theta)/\theta)$ term versus the pH will in general yield a straight line leveling off to constant initial and final pH values. The variation of the slope, n, in the course of the titration is indicative for the structural changes that might take place during the titration. For poly(acrylic acid) the slope is approximately constant. Poly(methacrylic acid) (PMA), however, shows a conformational transition, and in the Henderson–Hasselbalch plot an initial linear branch is gradually transformed into a final linear branch. An AB type model has been developed[42] in which the molar fractions of the initial and the final states are obtained from the linear regression results of these branches. An extension of this model is introduced here to analyze the ABC type transition. For completeness, we present here both the AB and the ABC analysis.

The AB Case. Consider the conformational transition A ⇄ B. One defines the *conformational* equilibrium constant as follows: $K = [B]/[A]$. For the pure states A and B the degree of dissociation of the protons can be defined by analogy with eq 1 as follows:

$$\alpha = \frac{K_{aA}}{[H^+] + K_{aA}} \tag{4a}$$

$$\beta = \frac{K_{aB}}{[H^+] + K_{aB}} \tag{4b}$$

K_{aA} and K_{aB} refer to the *proton dissociation* equilibrium constant K_a's of the pure A and B states, respectively. For each state a Henderson–Hasselbalch equation by analogy with eq 3 can also be constructed:

$$pH = pK_0^A - n_A \log\frac{1-\alpha}{\alpha} \tag{5a}$$

$$pH = pK_0^B - n_B \log\frac{1-\beta}{\beta} \tag{5b}$$

The values of pK_0^A, pK_0^B, n_A, and n_B can be obtained by regression of the linear branches as the slope and the intercept; e.g., see Figure 5. Next, from eqs 5a,b and the balance eqs 6a,b for charge neutrality and mass conservation, respectively,

$$\theta = \alpha f_A + \beta f_B \tag{6a}$$

$$f_A + f_B = 1 \tag{6b}$$

the expressions for the molar fractions of the products A and B, f_A and f_B can be defined

$$f_A = \frac{\theta - \beta}{\alpha - \beta} \tag{7a}$$

$$f_B = \frac{\theta - \alpha}{\beta - \alpha} \tag{7b}$$

If f_B is plotted against θ a composition curve of the "disordered state" is obtained. For the AB case, the shape of such a curve, as for PMA, will in general be sigmoidal with an approximately symmetric distribution around the point of inflection, which can be designated either T_m or θ_m, depending on which quantity is varied in the experiment. In the analysis of the titrations, we will consider the isothermal case in which the midpoint of transition is designated θ_m.

Since thermodynamic equilibrium holds for every θ, we can make use of the definition of the *conformational* equilibrium constant for the A ⇄ B transition: $K = [B]/[A] = f_B/f_A$, which can be calculated with eqs 7a,b. Note that K is a constant at every given degree of dissociation θ and it is a function of θ and temperature. The following physical interpretation of the dependence of K on θ can be given. If charge to the A state of the macromolecular chain, then the electrostatic energy of A is increased. The electrostatic repulsion of the charges becomes the driving force of the conformational transition to B if this transition can serve to escape from the unfavorable A state to a more "relaxed" B state in which the charges will be effectively more shielded and/or further apart. Thus, increasing the charge of the system will increase the change of free energy of the AB transition and hence increase the value of K.

From a plot of f_B/f_A versus θ of several titrations (not shown here) it appeared that K is an exponential function of θ. A plot of the logarithm of f_B/f_A versus θ gives a straight line which enables the determination of the value of θ for which $\ln(K)$ equals zero; this point identifies the midpoint of the transition, θ_m (cf. Figure 9). We will use this linear dependence of $\ln(K)$ on θ in the next section to extrapolate the values of K_1 and K_2 for the A ⇄ B and the B ⇄ C transitions under the assumption of uncoupled processes.

The ABC Case. Consider the two conformational transitions: A ⇄ B followed by B ⇄ C. One defines the *conformational* equilibrium constants as follows: $K_1 = [B]/[A]$ and $K_2 = [C]/[B]$. For the *proton dissociation* equilibria of the pure states A, B, and C we can define

expressions similar to eq 4 and again by analogy with eqs 1 and 3 the following Henderson–Hasselbalch equations hold.

$$\mathrm{pH} = \mathrm{p}K_0^{\mathrm{A}} - n_{\mathrm{A}} \log \frac{1-\alpha}{\alpha} \tag{8a}$$

$$\mathrm{pH} = \mathrm{p}K_0^{\mathrm{B}} - n_{\mathrm{B}} \log \frac{1-\beta}{\beta} \tag{8b}$$

$$\mathrm{pH} = pK_0^{\mathrm{C}} - n_{\mathrm{C}} \log \frac{1-\gamma}{\gamma} \tag{8c}$$

In the *uncoupled* case, i.e., if [A] > 0 then [C] = 0 and if [C] > 0 then [A] = 0, we can proceed as in the previous section and obtained two sets, namely, the AB and the BC cases. The AB expressions are again given by eqs 7a,b; the BC expressions read

$$f_{\mathrm{B}} = \frac{\theta-\gamma}{\beta-\gamma} \tag{9a}$$

$$f_{\mathrm{C}} = \frac{\theta-\beta}{\gamma-\beta} \tag{9b}$$

From the experimental Henderson–Hasselbalch curve, the parameters for A and C, the initial and the final branches, can be derived by linear regression. The parameters for the intermediate B state are obtained by an iterative procedure. The procedure starts with an estimate of the Henderson–Hasselbalch parameters for the B state such that a straight line in between the lines of A and C is obtained; cf. Figure 8. From these Henderson–Hasselbalch parameters of B, a first estimate of a set of β values is obtained for the entire range of the titration with eq 8b. There are several restricting conditions for this set of β solutions. Since we postulate B as an intermediate species and since the composition curve of Figure 7 (63 °C) indicates that for roughly $0.3 < \theta < 0.5$ the first, s-shaped process is dominant and that at $\theta > 0.5$ the second process begins, we can postulate that for $0.3 < \theta < 0.5$, $K_1 > K_2$ and $K_2 \approx 0$ and for $\theta > 0.5$, $K_1 > K_2 > 0$. With use of the definitions of K_1 and K_2 and eqs 7a,b and 9a,b and these criteria, one demands that in the region of the first transition, $\alpha < \theta < \beta < \gamma$ while in the second transition region, $\alpha < \beta < \theta < \gamma$. Once these conditions are satisfied, θ, α, and γ are known and a first consistent set of β values is obtained. Thus far, we have assumed *un*coupled processes. Now we introduce *coupling* in the model by taking into account the cross-term K_1K_2, since for the coupled ABC case, $K_1 = [\mathrm{B}]/[\mathrm{A}]$, $K_2 = [\mathrm{C}]/[\mathrm{B}]$, and $K_1K_2 = [\mathrm{C}]/[\mathrm{A}]$. To obtain the cross-term for the coupled case in the entire range of the titration, we must extrapolate the linear dependence of $\ln(K_i)$ on θ in the uncoupled case, which applies only to a limited range, to the entire range of the titration; cf. Figure 9. From the known values of θ, α, and γ and the first consistent set of β values, the molar fractions of A, B, and C in the *un*coupled case are calculated using expressions 7a,b and 9a,b and next K_1 and K_2 can be calculated. A linear regression of the logarithm of K_1 and K_2 plotted against θ enables the extrapolation. With use of these extrapolated values of K_1 and K_2, the molar fractions of A, B, and C in the coupled case are defined as follows:

$$f_{\mathrm{A}} = 1/D \tag{10a}$$

$$f_{\mathrm{B}} = K_1/D \tag{10b}$$

$$f_{\mathrm{C}} = K_1K_2/D \tag{10c}$$

$$D = 1 + K_1 + K_1K_2 \tag{10d}$$

In this case, the balance equations for charge neutrality and mass conservation for the ABC case read

$$\theta = \alpha f_{\mathrm{A}} + \beta f_{\mathrm{B}} + \gamma f_{\mathrm{C}} \tag{11a}$$

$$f_{\mathrm{A}} + f_{\mathrm{B}} + f_{\mathrm{C}} = 1 \tag{11b}$$

The molar fractions f_{A}, f_{B}, and f_{C} are then recalculated with eqs 10a–c, and from these new values and the known values of α and γ, the next estimate of β values can be obtained using eq 11a. Next, we use these β values to construct a new Henderson–Hasselbalch plot of $\log((1-\beta)/\beta)$ versus pH. A linear regression of this Henderson–Hasselbalch branch yields the new parameters $\mathrm{p}K_0^{\mathrm{B}}$ and n_{B}, and the procedure is repeated until the output equals the input. In Figure 9 the final solution is shown as the $\ln(K_i)$ versus θ plot, and in Figure 10 the final solution is shown as a set of composition curves of A, B, and C in the course of the titration. Both figures show the validity of the uncoupled approximation at the beginning and the end of the titration as well as the coupling of the two transitions by the development of f_{B}. At the end of the titration, the conversion to C is virtually complete, which shows the consistency of the solution.

The extrapolation method of $\ln(K_i)$ versus θ leads to an expression which enables an analytical determination of the midpoint of the ith transition, since at the midpoint $K = 1$ and $\ln(K_i) = 0$. In the ABC case this method is essential for the separate determination of the midpoints of the first and the second transitions.

Discussion

A Hypothesis for the Two Processes. (1) The First Transition. A tentative explanation for the first transition is offered by a mechanism in which the side chains gradually unfold from the backbone. In the literature, several authors have made suggestions for folding of the side chains around the backbone. The molecular models of xanthan sodium salt, i.e., at $\theta' = 1$, show that, although the side chains can fold around the backbone, a minimization of free energy is not correspondingly achieved.[11,51] The effect of gradually increasing the charge on the acidic form of the polymer however has not yet been included in the modeling.

If we consider the starting point of the titrations, then the side chains are practically uncharged (due to autodissociation, the lowest degree of dissociation is roughly 0.2) and folding around the backbone to form hydrogen-bonded structures may be favorable. Since the charge density is low, the repulsion is weak and the side chains may serve to dissolve the cellulosic backbone by covering it up. Upon increasing the charge, the electrostatic interaction counteracts the hydrogen bonding, which causes the side chains to unfold. Since the interaction is of short range and presumably intramolecular, a cooperative process is expected to occur which is not easily quenched by the addition of salt and which is reversible on a short time scale (~24 h[34]). Taking roughly 10 Å as a typical distance between side chains,[11,40] electrostatic screening is expected only if the Debye length is of the same order of magnitude which is achieved at roughly 100 mM of added salt. Indeed, in optical rotation experiments complete quenching of the transition is observed at this ionic strength.[26] At lower ionic strengths the transition is not quenched but shifted to higher values of T or θ, which is fully consistent with our titration results at 63 °C and C_s = 5–39 mM; cf. Figure 3. That such an unfolding process would lead to the observed changes of optical rotation and other observables can be understood since the chromophores and the majority of the polymer mass are situated in the side chains. The folded side chains will

make a contribution to the intrinsic persistence length, and if they cooperatively unfold, a much more flexible structure will emerge, in apparent agreement with the decrease of the viscosity in Figure 4. In recent NMR experiments[52] some evidence was found for enhanced mobility of the side chains in the premelting range, which is in agreement with our hypothesis.

(2) The Second Transition. The second transition, however, can be suppressed by the addition of a few mM of salt; with 5 mM salt added, the onset of the second transition is shifted beyond our experimental temperature range and it is estimated to take place at 70–75 °C. At this ionic strength, the Debye length is roughly 40 Å. At 0.5 mM, where the second transition is not quenched, the Debye length is roughly 90 Å. Thus, the length scale of the interaction which governs the second transition is of the order of 1–2 times the distance of one pitch of the helix (47 Å). A long-range intermolecular process such as the unraveling of a Rees type structure or the dissociation of helices, loops, and hairpins is likely to occur. These suggestions are in contrast with earlier postulations which exclude the possibility of loop formation in xanthan.[26] Whatever the nature of the second transition, it is obvious from the absence of the shear-thinning effect that a drastic change of the polymer structure must take place.

As mentioned above, in the literature the second transition of xanthan is not known. However, the influence of added salt on the conformational transition of a polyelectrolyte is known for DNA; see below.

A Comparison of the Second Transition with Experiments on DNA. For xanthan, transitions of the second kind are unprecedented in the literature. In a study of the temperature dependence of the UV absorption of a small self-complementary DNA dodecamer however, Marky et al.[53] observed a second transition following the well-known sigmoidal helix-to-coil transition. Their second transition was quenched by the addition of small amounts of salt with conservation of the first transition. These results were explained by assuming a salt-dependent equilibrium between dimer and hairpin formation.

Besides, in our opinion, the formation of a network-like structure of partly associated chains such as postulated for xanthan might be equally probable for DNA at low ionic strength since the double helix of DNA is known to denaturate, and a variety of partially interassociated chains are then perhaps formed. The dissociation of this network at higher temperatures may be an equally valid interpretation for the second transition as the melting of loops or hairpins.

Although in Marky's experiment a different parameter is varied, namely the temperature instead of the charge, the similarity of the composition curves of Marky's and our experiments may indicate that in both cases a transition of the second kind takes place, which makes the second transition perhaps a more general transition for polyelectrolyte solutions at low ionic strength.

Conclusions

In the analysis of the potentiometric titration curves, a new transition in addition to the sigmoidal transition is observed for aqueous solutions of native xanthan under low salt conditions.

With rotational viscosimetry the difference between the states after the two transitions was demonstrated. The difference of the length scales involved in both transitions may indicate that initially the side chains unfold cooperatively from the backbone and eventually the associated Rees type or hairpin-like structures dissociate or disentangle gradually. According to the similarity of the observations of the first transition in solutions of both sonicated and native xanthan, it can be concluded that for chains containing 1 to roughly 20 Kuhn segments the same transition takes place. A new empirical relation between the midpoints of the first transition, θ_m and T_m, is established, which may help to determine the phase diagram of the conformational transition of xanthan.

Acknowledgment. Mr. R. Visse of the Biochemistry Department of this laboratory is kindly thanked for his assistance with the biochemical purification method and the DNA and protein assay tests and stimulating discussions. The authors would like to express their gratitude to Dr. J. Brussee in the Department of Organic Chemistry of this laboratory for assistance with the optical rotation experiments and to Mr. B. van Haeringen for help with the OD and CD measurements performed at the Department of Biophysics of the Free University in Amsterdam. This work was supported by The Netherlands Foundation for Chemical Research (SON) with financial aid from The Netherlands Foundation for the Advancement of Pure Research (NWO).

References and Notes

(1) Jeanes, A.; Pittsley, J. E.; Senti, F. R. *J. Appl. Polym. Sci.* **1961**, *5*, 519.
(2) Jansson, P. E.; Kenne, L.; Lindberg, B. *Carbohydr. Res.* **1975**, *45*, 275.
(3) Melton, L. D.; Mindt, L.; Rees, D. A.; Sandersen, G. R. *Carbohydr. Res.* **1976**, *46*, 245.
(4) Sandford, P. A.; Pittsley, J. E.; Knutson, C. A.; Watson, P. R.; Cadmus, M. L.; Jeanes, A., Eds. *Extracellular Microbial Polysaccharides*; ACS Symposium Series 45; American Chemical Society: Washington, DC, 1977; pp 192–210.
(5) Holzwarth, G. *Biochemistry* **1976**, *15*, 4333.
(6) Whitcomb, P. J.; Ek, B. J.; Macosko, C. W., Eds. *Extracellular Microbial Polysaccharides*; ACS Symposium Series 45; American Chemical Society: Washington, DC, 1977; pp 160–173.
(7) Brawerman, G.; Mendecki, J.; Lee, S. Y. *Biochemistry* **1972**, *11*, 637.
(8) Sambrook, J.; Fritsch, E. F.; Maniatis, T. In *Molecular Cloning*; Cold Spring Harbor Laboratory Press: Cold Spring Harbor, NY, 1989.
(9) Morris, E. R.; Rees, D. A.; Young, G.; Wilkinshaw, M. D.; Darke, A. *J. Mol. Biol.* **1977**, *110*, 1.
(10) Moorhouse, R.; Wilkinshaw, M. D.; Arnott, S. *Extracellular Microbial Polysaccharides*; ACS Symposium Series 45; American Chemical Society: Washington, DC, 1977; pp 90–100.
(11) Okuyama, K.; Arnott, S.; Moorhouse, R.; Wilkinshaw, M. D.; Atkins, E. D. T.; Wolf-Ullish, Ch. *Fiber Diffraction Methods*; ACS Symposium Series 141; American Chemical Society: Washington, DC, 1980; pp 411–427.
(12) Holzwarth, G.; Prestridge, F. G. *Science (Washington, D.C.)* **1977**, *197*, 757.
(13) Stokke, B. T.; Smidsrød, O.; Elgsaeter, A. *Biopolymers* **1989**, *28*, 617.
(14) Milas, M.; Rinaudo, M. *Carbohydr. Res.* **1986**, *158*, 191.
(15) Norton, I. T.; Goodall, D. M.; Frangou, S. A.; Morris, E. R.; Rees, D. A. *J. Mol. Biol.* **1984**, *175*, 371.
(16) Paoletti, S.; Cesaro, A.; Delben, F. *Carbohydr. Res.* **1983**, *123*, 173.
(17) Cantor, C. R.; Schimmel, P. R. In *Biophysical Chemistry, Part 3: The Behavior of Biological Macromolecules*; W. H. Freeman: San Francisco, 1980; Chapter 22.
(18) Rees, D. A. *Biochem. J.* **1972**, *126*, 257.
(19) Holzwarth, G. *Carbohydr. Res.* **1978**, *66*, 173.
(20) Paradossi, G.; Brant, D. A. *Macromolecules* **1982**, *15*, 874.
(21) Sato, T.; Norisuye, T.; Fujita, H. *Polym. J.* **1984**, *16*, 341.
(22) Sho, T.; Sato, T.; Norisuye, T. *Biophys. Chem.* **1986**, *25*, 307.
(23) Zhang, L.; Liu, W.; Norisuye, T.; Fujita, H. *Biopolymers* **1987**, *26*, 333.
(24) Sato, T.; Norisuye, T.; Fujita, H. *Macromolecules* **1984**, *17*, 2696.
(25) Liu, W.; Norisuye, T. *Biopolymers* **1988**, *27*, 1641.
(26) Liu, W.; Sato, T.; Norisuye, T.; Fujita, H. *Carbohydr. Res.* **1987**, *160*, 267.
(27) Liu, W.; Norisuye, T. *Int. J. Biol. Macromol.* **1988**, *10*, 44.

(28) Lecourtier, J.; Chauveteau, G.; Muller, G. *Int. J. Biol. Macromol.* **1986**, *8*, 306.
(29) Muller, G.; Anrhourrache, M.; Lecourtier, J.; Chauveteau, G. *Int. J. Biol. Macromol.* **1986**, *8*, 167.
(30) Hacche, L.; Washington, G. E.; Brant, D. A. *Macromolecules* **1987**, *20*, 2179.
(31) Ross-Murphy, S. B.; Morris, V. J.; Morris, E. R. *Faraday Symp. Chem. Soc.* **1983**, *18*, 115.
(32) Jamieson, A. M.; Southwick, J. G.; Blackwell, J. *J. Polym. Sci., Polym. Phys. Ed.* **1982**, *20*, 1513.
(33) Carnali, J. O. *J. Appl. Polym. Sci.* **1991**, *43*, 929.
(34) Bezemer, L., et al., to be published.
(35) Odijk, T. J. *Macromolecules* **1979**, *12*, 688.
(36) Maret, G.; Milas, M.; Rinaudo, M. *Polym. Bull.* **1981**, *4*, 291.
(37) Sato, T.; Kakihara, T.; Teramoto, A. *Polymer* **1990**, *31*, 824.
(38) van Dijk, L.; Gruwel, M. L. H.; Jesse, W.; de Bleijser, J.; Leyte, J. C. *Biopolymers* **1987**, *26*, 261.
(39) Milas, M.; Rinaudo, M. *ACS Symp. Ser.* **1981**, *150*, 25–30.
(40) Zhang, L.; Takematsu, T.; Norisuye, T. *Macromolecules* **1987**, *20*, 2882.
(41) Nakasuga, M.; Norisuye, T. *Polym. J.* **1988**, *20*, 939.
(42) Leyte, J. C.; Mandel, M. *J. Polym. Sci., Part A* **1964**, *21*, 1879.
(43) Bradford, M. A. *Anal. Biochem.* **1976**, *72*, 248.
(44) Karsten, U.; Wollenberger, A. *Anal. Biochem.* **1972**, *46*, 135–148.
(45) Kennedy, J. F.; Bradshaw, I. J. *Br. Polym. J.* **1984**, *16*, 95.
(46) Bokma, J. T.; Johnson, W. C., jr.; Blok, Joh. *Biopolymers* **1987**, *26*, 893.
(47) Aust, N.; Meyer-Kolsthorn, U.; Schreiber, A.; Zugenmaier, P. *Angew. Makromol. Chem.* **1992**, *195*, 57.
(48) Sloneker, J. H.; Jeanes, A. *Can. J. Chem.* **1962**, *40*, 2067.
(49) Weast, R. C., Ed. *CRC Handbook of Chemistry and Physics*, 62nd ed.; CRC Press: Boca Raton, FL, 1981; p D-145.
(50) Viswanath, D. S.; Natarajan, G. In *Data book on the viscosity of liquids*; Hemisphere Publishing Corp.: Bristol, PA, 1989; p 457.
(51) Perez, S.; Vergelati, C. *Int. J. Biol. Macromol.* **1987**, *9*, 211.
(52) Gamini, A.; de Bleijser, J.; Leyte, J. C. *Carbohydr. Res.* **1991**, *220*, 33.
(53) Marky, L. A.; Blumenfield, K. S.; Kozlowski, S.; Breslauer, K. J. *Biopolymers* **1983**, *22*, 1247.